Structure, electrical and thermal properties of single-crystal BaCuGdTe3

Journal:	*Dalton Transactions*
Manuscript ID	DT-ART-04-2023-001192.R1
Article Type:	Paper
Date Submitted by the Author:	24-May-2023
Complete List of Authors:	Gunatilleke, Wilarachchige ; University of South Florida College of Arts & Sciences, Physics Wong-Ng, Winnie; NIST, Materials Measurement Science Chang, Tieyan; The University of Chicago, NSF's ChemMatCARS Chen, Yu-Sheng; The University of Chicago, Nolas, George; University of South Florida, Department of Physics

ARTICLE

Structure, electrical and thermal properties of single-crystal BaCuGdTe$_3$

Received 00th January 20xx,
Accepted 00th January 20xx

DOI: 10.1039/x0xx00000x

Wilarachchige D. C. B. Gunatilleke,[a] Winnie Wong-Ng,[b] Teiyan Chang,[c] Yu-Sheng Chen[c] and George S. Nolas*[a]

Single crystals of the quaternary chalcogenide BaCuGdTe$_3$ were obtained by direct reaction of elements allowing for a complete investigation of the intrinsic electrical and thermal properties of this previously uninvestigated material. The structure was investigated by high-resolution single-crystal synchrotron X-ray diffraction, revealing an orthorhombic crystal structure with the space group *Cmcm.* Although recently identified as a semiconductor suitable for thermoelectric applications from theoretical analyses, our electrical resistivity and Seebeck coefficient measurements show metallic conduction, the latter revealing strong phonon-drag. Temperature dependent hole mobility reveals dominant acoustic phonon scattering. Heat capacity data reveal a Debye temperature of 183 K and a very high density of states at the Fermi level, the latter confirming the metallic nature of this composition. Thermal conductivity is relatively high with Umklapp processes dominating thermal transport above the Debye temperature. The findings in this work lay the foundation for a more detailed understanding of the physical properties of this and similar multinary chalcogenide materials, and is part of the continuing effort in investigating quaternary chalcogenide materials and their suitability for use in technological applications.

Introduction

Research into new materials and compositions, as well as an understanding of their physical properties, is critical in advancing technological fields of interest and enhancing device development for these applications. One class of materials that continues to be of great interest are transition metal chalcogenides, whether binary or multinary compositions[1,2]. In the case of binaries, this is partly due to the interest in 2D materials and their interesting properties with potential for applications including topological insulators[3,4], magnetoresistance[5], superconductivity[6] and ferromagnetism[7,8]. However, multinary chalcogenides are of interest for applications such as photovoltaics[9–13], thermoelectrics[14–18], and non-linear optics[19–22]. Several compositions can be synthesized with non-toxic and earth-abundant constituents, which is of particular interest for device development.

One class of quaternary chalcogenides that is of current interest are AMM'Q$_3$, where A is an alkali or alkali earth metal, M is a transition metal, M' is a lanthanide or transition metal and Q is a chalcogen. These materials have been known for three decades[23], Ibers and co-workers having enumerated over 150 different compositions forming in three different structure types[24]. Most recently several hundred different compositions have been reported as stable by employing high-throughput density functional theory calculations[25]. Furthermore, there is a current strong interest in specific compositions for thermoelectric applications, as certain compositions have been predicted to possess low thermal conductivity[25–28]. Many of the initial theoretical investigations on AMM'Q$_3$ compounds predicted semiconducting behavior. K. Pal *et al.* reported that BaAgYTe$_3$ and BaCuYTe$_3$ may be suitable thermoelectric materials due to calculations indicating low lattice thermal conductivity[26,27]. In addition, theoretical investigations predicted BaCuGdTe$_3$ to be a semiconductor and a potential candidate for thermoelectric applications[29]. However, BaCuScTe$_3$ was revealed to be a poor metal even though semiconducting properties were predicted[30]. The crystal structures of all of the above-mentioned compositions belong to the orthorhombic *Cmcm* space group. In these structure types the lanthanide and transition metals have a direct impact on the electronic properties of these materials, therefore the specific stoichiometry also affects the assessment of these materials for thermoelectric applications. Nevertheless, it is noteworthy that there are scarce reports on the experimental transport properties for this large class of materials. Motivated by our continuing interest in quaternary chalcogenides as well as their physical properties for energy related applications, we investigated the structure, temperature-dependent transport properties and specific heat of BaCuGdTe$_3$, a member of AMM'Q$_3$ family of compounds that forms in the orthorhombic

---

[a] Department of Physics, University of South Florida, Tampa, FL 33620, USA
[b] Materials Measurement Science Division, National Institute of Standards and Technology, Gaithersburg, MD 20899, USA
[c] ChemMatCARS, University of Chicago, Argonne, IL 60439, USA
*E-mail: gnolas@usf.edu

Cmcm space group. Specifically, we grew single crystals and investigated the resistivity, *ρ*, Seebeck coefficient, *S*, Hall, R_h, thermal conductivity, *κ*, and isobaric heat capacity, *C*p. To the best of our knowledge, there is no previous report on measured physical properties of this composition.

Experimental

Single crystals of $BaCuGdTe_3$ were grown by direct reaction of the constituent elements. In a glovebox with a N_2 atmosphere, Ba pieces (99.2%, Alfa Aesar), Cu powder (99.9%, Alfa Aesar), Gd pieces (99.9999%, Ames Laboratories) and Te powder (99.8%, Acros Organics) were combined in 1:1:1:3 stoichiometric ratio in a silica ampoule and placed in a quartz tube. The quartz tube was sealed under vacuum before being placed in a resistive furnace. It was then heated to 1173 K within 48 hours and held at this temperature for 96 hours at which point it was slowly cooled to 673 K at 2.5 K/hr. The cooling rate was subsequently increased to 32 K/hr to bring the reaction mixture to room temperature. Rounded cuboid shaped dark single crystals were extracted from the resultant specimen under an optical microscope for structure characterization.

Single-crystal X-ray diffraction (XRD) measurements were conducted at NSF's ChemMatCARS, Sector 15 of the Advanced Photon Source of Argonne National Laboratory. Data collection was accomplished using a Huber 3-axis diffractometer with a Pilatus3 X 2M CdTe detector[31]. Using Olex2[32], the structure was solved with the XT[33] structure solution program using Intrinsic Phasing and refined with the XL[34] refinement package. An approximately 0.7 x 0.7 x 1.0 mm^3 crystal was used for the measurement of electrical and thermal properties from 300 K to 20 K using a custom-built radiation-shielded vacuum probe[35,36] with a maximum experimental uncertainty of 20% associated with determination of the geometrical dimensions of the crystal. We have previously measured crystal of this, and smaller, size and employed similar procedures to that previously reported.[37-40] Low-temperature $\boldsymbol{C_p}$ data was measured using the heat capacity (HC) option on a commercial Quantum Design Physical Property Measurement System using the thermal N-grease accompanied by appropriate addenda. The maximum experimental uncertainty in the entire temperature range was estimated to be ± 6 %. Temperature dependent 4-probe Hall measurements were conducted using the resistivity option at multiple magnetic fields with a maximum field of 2.4 T. A measurement sequence was set up to alternate the direction of the magnetic field at each field.

Results and discussion

The single crystal refinement data are shown in Table 1. The atomic

Table 1. Crystal data and structure refinement.

Empirical formula	$BaCuGdTe_3$
Formula weight/gmol^{-1}	740.93
Temperature/K, Radiation	100.15, Synchrotron (λ = 0.49594 Å)
Crystal system, Space group	Orthorhombic, *Cmcm*
a/Å	4.4204(5)
***b*/Å**	14.693(2)
***c*/Å**	11.3601(12)
Volume/Å^3	737.84(14)
Z	4
ρ_{calc} g/cm^3	6.670
μ/mm^{-1}	10.725
F(000)	1220
Crystal size/mm^3	0.025 × 0.025 × 0.01
Diffractometer	Huber 3-circles diffractometer
2*θ* range for data collection/°	2.50 to 38.58
Index ranges	$-5 \leq h \leq 5$, $-19 \leq k \leq 19$, $-15 \leq l \leq 15$
Reflections collected	9699
Completeness to *θ*=17.311°	100.0%
Independent reflections	536 [R_{int} = 0.1045]
Data/restraints/parameters	536/0/25
Goodness-of-fit on F^2	1.026
Final R indexes [I ≥ 2σ (I)]	$R_1 = 0.0436$, $wR_2 = 0.1086$

Largest diff. peak/hole / e Å^{-3}	2.77/-2.55

coordinates and the isotropic (U_{eq}) and anisotropic displacement parameters (U_{ij}) are shown in Tables 2 and 3, respectively, with selected bond lengths given in Table 4. Our structure analyses indicated that $BaCuGdTe_3$ belongs to the Type II ($AMM'Q_3$) category[41]. The structure is orthorhombic, space group *Cmcm*, with lattice parameters *a* = 4.4204(5) Å, *b* = 14.693(2) Å and *c* = 11.3601(12) Å. $BaCuGdTe_3$ can be viewed as having a two-dimensional structure with parallel [$MM'Te_3$] slabs of alternating distorted $CuTe_4$ tetrahedra and $GdTe_6$ octahedra extending in the *ab* plane. These slabs are separated from each other by Ba atoms. Figure 1 illustrates the crystal structure and provides a perspective of the polyhedral view of the corner-shared $GdTe_6$ connected by $CuTe_4$ tetrahedra along the *ab* plane. Within the slab, the tetrahedral-tetrahedral, and octahedral-octahedral polyhedra are corner sharing, whereas the octahedral-tetrahedral polyhedra are edge-sharing. The Cu-Te bond lengths are similar to those of $NaCuZrTe_3$[42], and the Gd-Te bond lengths are similar to those of $CsZnGdTe_3$ [43]. The tetrahedral Te-Cu-Te and octahedral Te-Gd-Te angles deviate only slightly from the ideal tetrahedral angle of 109.47° and octahedral angles of 90° or 180°, respectively. Our structural data are in good agreement with that reported by Prakash *et al.* [44].

To investigate the electrical properties, temperature dependent ρ, S and R_h were measured. Measurements in two arbitrary directions perpendicular to each other on different single crystals gave the same results. As shown in Figure 2, ρ increases with increasing temperature indicative of metallic behavior, with values comparable to that of other intermetallic compounds such as $GdAl_2$ and $TbAl_2$ [45]. At the lowest measured temperatures $d\rho/dT > 0$ indicating that the residual resistivity is not yet reached. Nevertheless, the relatively high residual resistance ratio (RRR ≈ 5) is comparable to that reported for single crystal metallic clathrate compositions as well as other ternary and quaternary chalcogenides [46–52], and indicative of a good quality single crystal. We also considered the possibility that defects may affect the transport properties; however, our single crystal structure refinements show no fractional occupancy on any of the crystallographic positions. Hence, we conclude that the metallic behavior is intrinsic to $BaCuGdTe_3$. We note that orthorhombic $BaCuScTe_3$ was also reported to be a metal[30]. As shown in Figure 3, all measured S values are positive for the entire measure temperature range indicating that holes are the majority carriers. The peak at approximately 60 K indicates strong phonon drag, an effect that is a significant contributor to S in pure metallic elements such as Cu and Ag, as well as for rare earth intermetallic binaries such as $GdCu_2$ and $TbCu_2$ [45,53]. The solid line in the inset to Figure 3 is a linear fit of the form $\boldsymbol{S = aT + bT^3}$, where the first and the second terms represent diffusion and phonon-drag contribution to S, respectively. From the

Table 2. Atomic coordinates and equivalent* isotropic atomic displacement parameters (Å^2).

Atom	*x/a*	*y/b*	*z/c*	U_{eq} *	Atomic occupancy	# positions
Gd	0.5	0.5	0.5	0.0134(4)	1.0	4*a*
Ba	0	0.2505(1)	0.75	0.0143(4)	1.0	4*c*
Cu	0	0.5324(2)	0.75	0.0166(7)	1.0	4*c*
Te1	0.5	0.4290(1)	0.75	0.0127(4)	1.0	4*c*
Te2	0	0.6393(1)	0.9385(12)	0.0134(4)	1.0	8*f*

* U_{iso} is defined as one third of the trace of the orthogonalized U_{ij} tensor.

Table 3. Anisotropic Displacement Parameters (Å^2).

Atom	U_{11}	U_{22}	U_{33}	U_{23}	U_{13}	U_{12}
Gd	0.0088(6)	0.0135(6)	0.0180(7)	-0.0003(5)	0	0
Ba	0.0082(7)	0.0141(8)	0.0207(8)	0	0	0
Cu	0.0143(14)	0.0183(15)	0.0171(15)	0	0	0
Te1	0.0086(8)	0.0130(8)	0.0167(9)	0	0	0
Te2	0.0088(6)	0.0132(6)	0.0183(6)	0.0002(5)	0	0

* The anisotropic atomic displacement factor exponent takes the form: $-2\pi^2$ [$h^2a^{*2}U_{11}$ +... + $2hka^*b^*U_{12}$]

Table 4. Selected bond lengths.

Bond Length (Å)

Gd-Te1	3.0256(7)
Gd-Te2	3.0920(9)
Cu-Te1	2.682(2)
Cu-Te2	2.655(2)
Ba-Te1	3.430 (2)
Ba-Te2	3.4844(12)

data fit the phonon-drag contribution, S_g = - 0.014T^3 μV/K, is significantly lower than the values reported for Cu-Al alloys[54]. This effect is suppressed with increasing temperature as diffusion dominates at higher temperatures, leading to a steady increase in S with increasing temperature. The temperature dependent Hall, R_h, decreases with increasing temperature as shown in Figure 4. Near room temperature, the data becomes nearly temperature-independent with a hole concentration of 5 x 10^{20} cm^{-3} at 300 K. The inset to Figure 4 shows temperature dependent hole mobility, μ_h. The solid line represents a $T^{-3/2}$ dependance indicative of acoustic phonon scattering. A hole effective mass, m^*, of 0.3m_e obtained at 300 K is lower than that of $Cu_2MnSnSe_4$ [55]and $Cu_2ZnSnSe_4$[56] and comparable with calculated m^* for $TlCuZrSe_3$ and $BaCuYTe_3$[27].

Low κ values have been calculated for certain compositions in the AMM'Q_3 family of compounds, thus their interest as potential for thermoelectric applications. The alignment of $CuTe_4$ tetrahedra and $GdTe_6$ octahedra into polyhedral slabs in $BaCuGdTe_3$ can presumably affect both the electronic and thermal properties of this material with the presence of lone pair electrons on tellurium [30], as reported for other quaternary chalcogenide compositions [57,58]. To investigate the thermal properties of this material, we measured the low temperature C_p, as shown in Figure 5. The Dulong-Petit limit is achieved near 200 K indicating the majority of acoustic and optic mode frequencies are excited above this temperature.

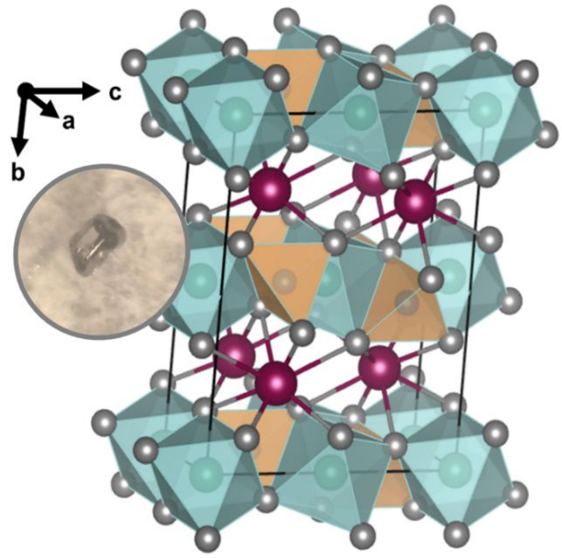

Figure 1. The crystal structure of $BaCuGdTe_3$. The layers of $GdTe_6$ (light green) and $CuTe_4$ (light orange) polyhedra with metal atoms in their center in the *ab* plane are connected by Ba (Red) atoms. Unit cell boundaries are marked by solid black lines. An image of the single crystal is also displayed.

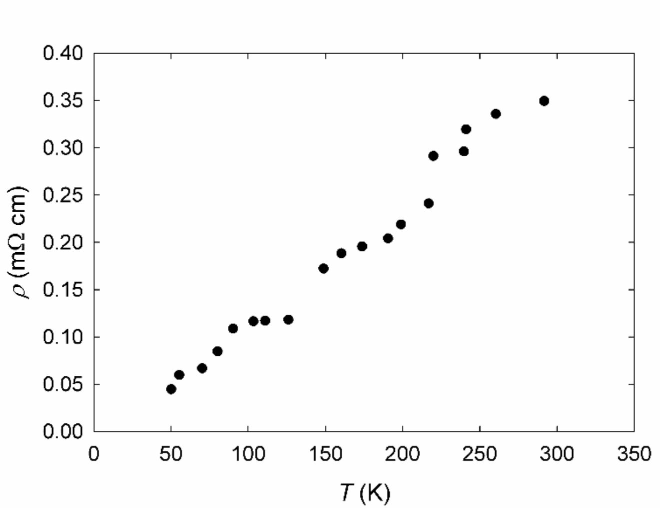

Figure 2. Temperature dependent ρ data.

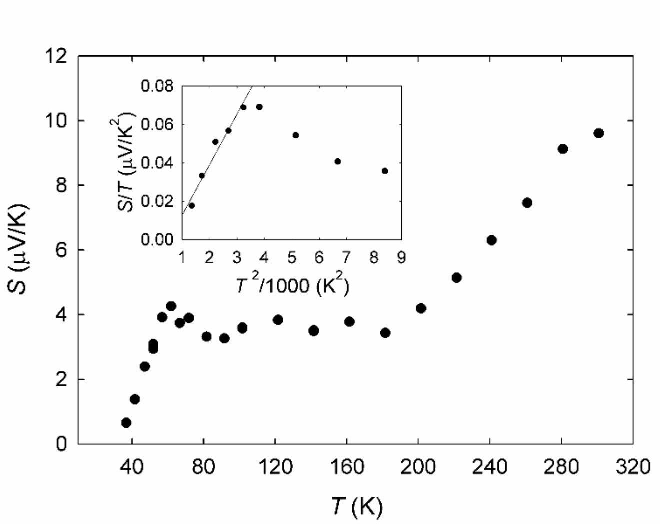

Figure 3. Temperature dependent S with the inset showing S/T vs T^2 at low temperatures, where the solid line is a fit of the form $S/T = a + bT^2$.

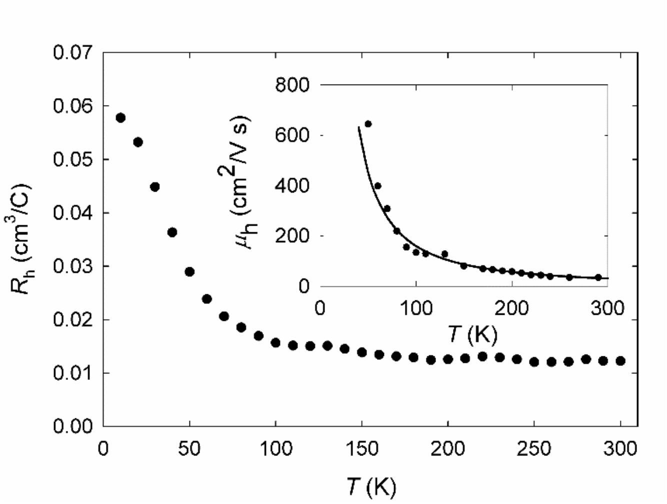

Figure 4. Temperature dependent R_h data. The inset shows temperature dependent μ_h with the solid line representing $T^{-3/2}$ dependence corresponding to acoustic phonon scattering.

The solid line in the inset of Figure 5 is a low temperature linear fit to the data of the form, $\boldsymbol{C_p = \gamma T + \beta T^3}$, where the first and second terms represent the Sommerfeld coefficient and the lattice contribution, respectively [59]. Using the lattice contribution from the data fit, $\boldsymbol{\beta = 1.8\ \mathrm{mJ\ mol^{-1}K^{-4}}}$, the Debye temperature, $\boldsymbol{\theta_D}$, can be determined from the low temperature C_p data using the relation $\boldsymbol{\theta_D = (12\pi^4 R n_a/5\beta)^{1/3}}$, where $\boldsymbol{n_a}$ is number of atoms per formula unit, and R is the universal gas constant. A value of 183 K thus obtained for $\boldsymbol{\theta_D}$ is in good agreement with the Dulong-Petit limit observed at high temperatures. The relatively high value of the Sommerfeld coefficient, $\boldsymbol{\gamma = 11.8\ \mathrm{mJ\ mol^{-1}K^{-2}}}$, obtained from our data fit corroborates the metallic nature of this material. Temperature dependent κ data for $BaCuGdTe_3$ are shown in Figure 6. The material displays relatively large κ over the entire measured temperature range, higher than that for $BaCuScTe_3$ at 300 K[30]. The electronic contribution to κ, $\kappa_E = LT/\rho$, was estimated using the value of 2.44 x.10^{-8} V^2/K^2 for Lorentz number, L. The contribution from κ_E is relatively small (24% of κ at 300 K) for a metal and decreases with increasing temperature as expected. However, κ increases with increasing temperature up to approximately 180 K after which κ shows a 1/T dependence indicative of Umklapp scattering, as shown in Figure 6. Although $BaCuGdTe_3$ displays metallic behavior at low temperatures, κ decreases with increasing temperature above $\boldsymbol{\theta_D}$. This is in line with the relatively temperature independent behavior of R_h above $\boldsymbol{\theta_D}$, and indicates no further contributions to thermal transport from the charge carriers. The distorted $CuTe_4$ tetrahedra and $GdTe_6$ octahedra extending in the *ab* plane in the crystal structure of $BaCuGdTe_3$, as discussed above, presumably contributes to the temperature dependent behavior of κ, as in the case of BiAgOSe[60].

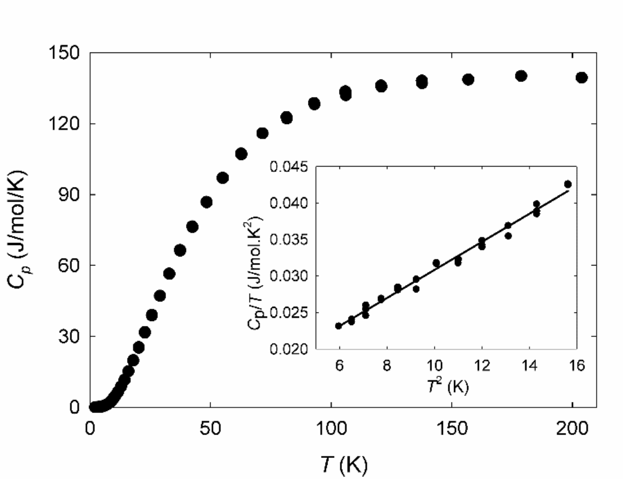

Figure 5. Temperature dependent C_p with the inset showing C_p/T vs T^2 at low temperatures, where the solid line is a fit of the form $C_p/T = \gamma + \beta T^2$.

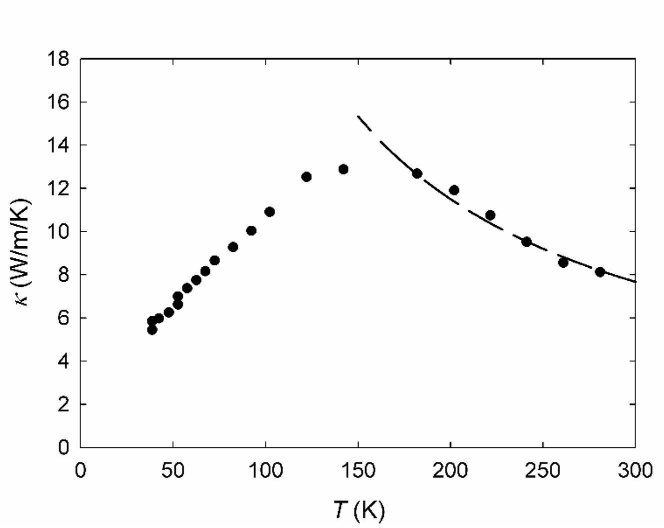

Figure 6. Temperature dependent κ data. The dashed line represents the 1/T dependence above $\boldsymbol{\theta_D}$.

Although $BaCuGdSe_3$ is a semiconductor with a relatively large bandgap[61], the tellurium composition shows metallic behavior. A similar scenario has been reported for the p-type semiconductor $BaCuScSe_3$ and metallic $BaCuScTe_3$[30]. It should therefore be of interest to investigate other $KCuZrS_3$ type layered structure AMM'Q_3 compositions as this will aid in the fundamental understanding of these relatively unexplored but technologically important class of materials.

Conclusions

Experimental electrical and thermal properties of $BaCuGdTe_3$ are reported for the first time. Temperature dependent ρ indicates metallic behavior with S data indicating significant phonon drag up to 60 K. Investigations into temperature dependent Hall revealed acoustic phonon scattering affecting electronic transport. Low temperature C_p measurements revealed a Debye temperature of 183 K, and a very high density of states at the Fermi level indicating metallic behavior corroborated by the relatively high κ observed for this material. With a majority of the predicted thermodynamically stable AMM'Q_3 compositions yet to be investigated, these results contribute to the fundamental understanding of these and related materials of current interest for technologically important applications.

Author Contributions

Wilarachchige D. C. B. Gunatilleke: investigation, formal analysis, visualization, writing – original draft. Winnie Wong-Ng: data curation, formal analysis. Teiyan Chang: data curation. Yu-Sheng Chen: data curation, formal analysis. George S. Nolas: conceptualization, investigation, supervision, writing – original draft, project administration.

Conflicts of interest

There are no conflicts to declare.

Acknowledgements

This work was supported, in part, by the National Science Foundation, Grant No. DMR-1748188. The authors acknowledge ChemMatCARS Sector 15 which is principally supported by the National Science Foundation/Department of Energy under grant number NSF/CHE- 1834750. Use of the Advanced Photon Source was supported by the U. S. Department of Energy, Office of Science, Office of Basic Energy Sciences, under Contract No. DE-AC02-06CH11357.

References

1 K. Mitchell and J. A. Ibers, *Chem. Rev.*, 2002, **102**, 1929–1952.
2 S.-L. Li, K. Tsukagoshi, E. Orgiu and P. Samorì, *Chem. Soc. Rev.*, 2015, **45**, 118–151.
3 J. Zhao, S. M. Islam, S. Hao, G. Tan, C. C. Stoumpos, C. Wolverton, H. Chen, Z. Luo, R. Li and M. G. Kanatzidis, *J. Am. Chem. Soc.*, 2017, **139**, 12601–12609.
4 J. J. Cha, K. J. Koski and Y. Cui, *Phys. Status Solidi RRL – Rapid Res. Lett.*, 2013, **7**, 15– 25.
5 A. P. Ramirez, R. J. Cava and J. Krajewski, *Nature*, 1997, **386**, 156–159.
6 W. Shi, J. Ye, Y. Zhang, R. Suzuki, M. Yoshida, J. Miyazaki, N. Inoue, Y. Saito and Y. Iwasa, *Sci. Rep.*, 2015, **5**, 12534.
7 M. Sturza, J. M. Allred, C. D. Malliakas, D. E. Bugaris, F. Han, D. Y. Chung and M. G. Kanatzidis, *Chem. Mater.*, 2015, **27**, 3280–3290.
8 M. Bonilla, S. Kolekar, Y. Ma, H. C. Diaz, V. Kalappattil, R. Das, T. Eggers, H. R. Gutierrez, M.-H. Phan and M. Batzill, *Nat. Nanotechnol.*, 2018, **13**, 289–293.
9 G. S. Nolas, M. S. Hassan, Y. Dong and J. Martin, *J. Solid State Chem.*, 2016, **242**, 50– 54.
10 S. K. Wallace, D. B. Mitzi and A. Walsh, *ACS Energy Lett.*, 2017, **2**, 776–779.
11 W. Wang, M. T. Winkler, O. Gunawan, T. Gokmen, T. K. Todorov, Y. Zhu and D. B. Mitzi, *Adv. Energy Mater.*, 2014, **4**, 1301465.
12 S. Palchoudhury, K. Ramasamy and A. Gupta, *Nanoscale Adv.*, 2020, **2**, 3069–3082.
13 Z. Wang, J. Cai, Q. Wang, S. Wu and J. Li, *Npj Comput. Mater.*, 2021, **7**, 1–11.
14 F. Gascoin and A. Maignan, *Chem. Mater.*, 2011, **23**, 2510–2513.
15 U. Aydemir, J.-H. Pöhls, H. Zhu, G. Hautier, S. Bajaj, Z. M. Gibbs, W. Chen, G. Li, S. Ohno, D. Broberg, S. Dongmin Kang, M. Asta, G. Ceder, M. Anne White, K. Persson, A. Jain and G. Jeffrey Snyder, *J. Mater. Chem. A*, 2016, **4**, 2461–2472.
16 Y. Dong, H. Wang and G. S. Nolas, *Phys. Status Solidi RRL – Rapid Res. Lett.*, 2014, **8**, 61–64.
17 K. Wei, L. Beauchemin, H. Wang, W. D. Porter, J. Martin and G. S. Nolas, *J. Alloys Compd.*, 2015, **650**, 844–847.
18 K. Wei and G. S. Nolas, *ACS Appl. Mater. Interfaces*, 2015, **7**, 9752–9757.
19 M. E. Maldonado, A. Das, A. M. Jawaid, A. J. Ritter, R. A. Vaia, D. A. Nagaoka, P. G. Vianna, L. Seixas, C. J. S. de Matos, A. Baev, P. N. Prasad and A. S. L. Gomes, *ACS Photonics*, 2020, **7**, 3440–3447.
20 M.-Y. Li, Z. Ma, B. Li, X.-T. Wu, H. Lin and Q.-L. Zhu, *Chem. Mater.*, 2020, **32**, 4331– 4339.
21 I. Chung and M. G. Kanatzidis, *Chem. Mater.*, 2014, **26**, 849–869.
22 M. Piasecki, G. Myronchuk, O. Y. Khyzhun, A. Fedorchuk, B. Andryievsky, I. Barchyi and M. Brik, *J. Alloys Compd.*, 2022, **909**, 164636.
23 M. F. Mansuetto, P. M. Keane and J. A. Ibers, *J. Solid State Chem.*, 1992, **101**, 257–264.
24 L. A. Koscielski and J. A. Ibers, *Z. Für Anorg. Allg. Chem.*, 2012, **638**, 2585–2593.
25 K. Pal, Y. Xia, J. Shen, J. He, Y. Luo, M. G. Kanatzidis and C. Wolverton, *Npj Comput. Mater.*, 2021, **7**, 1–13.
26 K. Pal, Y. Xia, J. He and C. Wolverton, *Chem. Mater.*, 2019, **31**, 8734–8741.
27 K. Pal, X. Hua, Y. Xia and C. Wolverton, *ACS Appl. Energy Mater.*, 2020, **3**, 2110–2119.
28 K. Pal, Y. Xia, J. He and C. Wolverton, *Phys. Rev. Mater.*, 2019, **3**, 085402.
29 K. Eickmeier, R. Poschkamp, R. Dronskowski and S. Steinberg, *Eur. J. Inorg. Chem.*, 2022, **2022**, e202200360.
30 M. Ishtiyak, S. Jana, R. Karthikeyan, M. Ramesh, B. Tripathy, S. K. Malladi, M. K. Niranjan and J. Prakash, *Inorg. Chem. Front.*, 2021, **8**, 4086–4101.
31 The purpose of identifying the equipment and software in this article is to specify the experimental procedure. Such identification does not imply recommendation or endorsement by the National Institute of Standards and Technology.
32 O. V. Dolomanov, L. J. Bourhis, R. J. Gildea, J. a. K. Howard and H. Puschmann, *J. Appl. Crystallogr.*, 2009, **42**, 339–341.
33 G. M. Sheldrick, *Acta Crystallogr. Sect. Found. Adv.*, 2015, **71**, 3–8.
34 G. M. Sheldrick, *Acta Crystallogr. A*, 2008, **64**, 112–122.
35 J. Martin and G. S. Nolas, *Rev. Sci. Instrum.*, 2016, **87**, 015105.
36 J. Martin, S. Erickson, G. S. Nolas, P. Alboni, T. M. Tritt and J. Yang, *J. Appl. Phys.*, 2006, **99**, 044903.
37 S. Stefanoski, J. Martin and G. S. Nolas, *J. Phys. Condens. Matter*, 2010, **22**, 485404.
38 S. Stefanoski and G. S. Nolas, *Cryst. Growth Des.*, 2011, **11**, 4533–4537.
39 S. Stefanoski, Y. Dong and G. S. Nolas, *J. Solid State Chem.*, 2013, **204**, 166–169.
40 W. D. C. B. Gunatilleke, K. Wei, Z. Niu, L. Wojtas, G. Nolas and S. Ma, *Dalton Trans.*, 2017, **46**, 13342–13344.
41 Y. Liu, L. Chen, L.-M. Wu, G. H. Chan and R. P. Van Duyne, *Inorg. Chem.*, 2008, **47**, 855–862.
42 M. F. Mansuetto, P. M. Keane and J. A. Ibers, *J. Solid State Chem.*, 1993, **105**, 580–587.
43 J. Yao, B. Deng, L. J. Sherry, A. D. McFarland, D. E. Ellis, R. P.

Van Duyne and J. A. Ibers, *Inorg. Chem.*, 2004, **43**, 7735–7740.

44 J. Prakash, A. Mesbah, J. C. Beard and J. A. Ibers, *Z. Für Anorg. Allg. Chem.*, 2015, **641**, 1253–1257.

45 E. Gratz and M. J. Zuckermann, *J. Magn. Magn. Mater.*, 1982, **29**, 181–191.

46 M. A. Avila, D. Huo, T. Sakata, K. Suekuni and T. Takabatake, *J. Phys. Condens. Matter*, 2006, **18**, 1585.

47 M. Beekman, W. Schnelle, H. Borrmann, M. Baitinger, Yu. Grin and G. S. Nolas, *Phys. Rev. Lett.*, 2010, **104**, 018301.

48 S. Stefanoski, Y. Dong and G. S. Nolas, *J. Solid State Chem.*, 2013, **204**, 166–169.

49 C. L. Condron, S. M. Kauzlarich and G. S. Nolas, *Inorg. Chem.*, 2007, **46**, 2556–2562.

50 M. Boubeche, N. Wang, J. Sun, P. Yang, L. Zeng, S. Luo, Y. He, J. Yu, M. Wang, J. Cheng and H. Luo, *J. Phys. Condens. Matter*, 2022, **34**, 205602.

51 M. Boubeche, N. Wang, J. Sun, P. Yang, L. Zeng, Q. Li, Y. He, S. Luo, J. Cheng, Y. Peng and H. Luo, *Supercond. Sci. Technol.*, 2021, **34**, 115003.

52 A. Schlechte, R. Niewa, M. Schmidt, G. Auffermann, Y. Prots, W. Schnelle, D. Gnida, T. Cichorek, F. Steglich and R. Kniep, *Sci. Technol. Adv. Mater.*, 2007, **8**, 341.

53 I. Weinberg, *Phys. Rev.*, 1966, **146**, 486–489.

54 I. Weinberg, *Phys. Rev.*, 1965, **139**, A838–A843.

55 T. Wang, T. Huo, H. Wang and C. Wang, *Sci. China Mater.*, 2020, **63**, 8-15.

56 Y. Zhu, Y. Liu , X. Tan , G. Ren , M. Yu , T. Hu , A. Marcelli and W. Xu , *AIP Adv.*, 2018, **8** , 045218.

57 Y. Dong, A. R. Khabibullin, K. Wei, J. R. Salvador, G. S. Nolas and L. M. Woods, *ChemPhysChem*, 2015, **16**, 3264–3270.

58 J. Li, S. Hao, S. Qu, C. Wolverton, J. Zhao and Y. Wang, *Inorg. Chem.*, 2021, **60**, 325–333.

59 C. Kittel and P. McEuen, *Introduction to Solid State Physics*, John Wiley & Sons, 2018.

60 C. Zhang, J. He, R. McClain, H. Xie, S. Cai, L. N. Walters, J. Shen, F. Ding, X. Zhou, C. D. Malliakas, J. M. Rondinelli, M. G. Kanatzidis, C. Wolverton, V. P. Dravid and K. R. Poeppelmeier, *J. Am. Chem. Soc.*, 2022, **144**, 2569–2579.

61 F. Q. Huang, K. Mitchell and J. A. Ibers, *Inorg. Chem.*, 2001, **40**, 5123–5126.